1

Friction stir processing for architectured materials

Aude Simar and Marie-Noëlle Avettand-Fènoël

[1] Université catholique de Louvain, Institute of Mechanics, Materials and Civil Engineering (iMMC), Louvain-la-Neuve, Belgium aude.simar@uclouvain.be
[2] Université Lille 1, Unité Matériaux Et Transformations, UMR CNRS 8207, 59655 Villeneuve dAscq, France
Marie-Noelle.Avettand-Fenoel@univ-lille1.fr

Abstract. Friction Stir Processing (FSP) is a solid-state process derived from Friction Stir Welding (FSW). FSP may be applied for the efficient manufacturing of metallic alloys based architectured materials. Indeed, the FSP tools allow locally modifying the microstructure of alloys or assembling dissimilar materials. The architectured materials that were or may be manufactured by friction stir processing will be discussed in this chapter. FSP may improve the mechanical performances of cast alloys, process metal matrix composites (MMC), make sandwiches, foams or additively manufactured structures. The aim is to process materials with improved lightweight performances, static or fatigue properties, crack resistance, toughness or wear resistance.

1.1 Friction Stir Processing for architectured materials

Friction stir processing (FSP) is a solid-state process derived from an innovative welding process patented by TWI in 1991 called Friction stir welding (FSW) [1–3]. It uses a non-consumable tool with complex features favoring the mixing of material in the solid state. A rotating tool is mounted on a machine similar to a milling machine. This tool is composed of a pin and a shoulder (Fig. 1.1). It is introduced into the material along the joint axis until the shoulder gets in contact with the upper surface of the workpiece to process. The tool is then travelling forward with the shoulder remaining in contact with the upper surface of the workpiece. The side where the rotational tool movement is in the same direction as the advancing movement is called the advancing side (AS) and the opposite side is called the retreating side (RS) (Fig. 1.1). Heat generated by friction and deformation brings the material into a malleable state that promotes the material flow from the front to the back of the tool and around the pin where it cools down. The temperatures

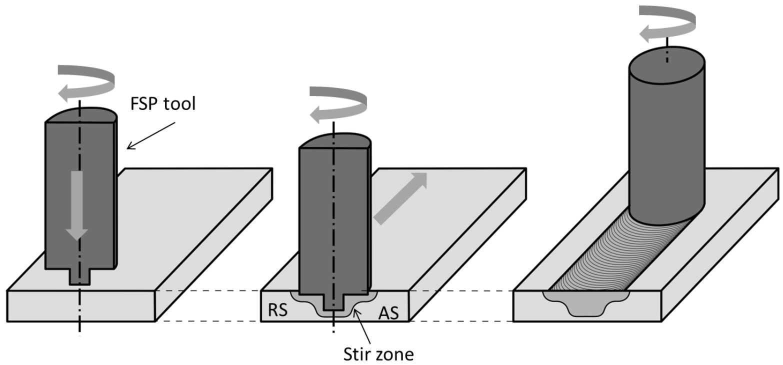

Fig. 1.1. Principle of Friction Stir Processing (FSP). RS = Retreating Side, AS = Advancing Side (Schematic by N. Jimenez-Mena)

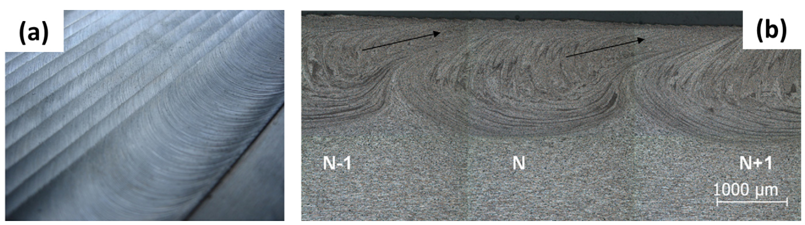

Fig. 1.2. Multipass surface modification of an Al5083-H111 by FSP. (a) Surface finish (b) Multiple adjacent stir zones (or nugget zone). From Gandra *et al.* [6].

reached are typically of 0.6-0.9 times the melting temperature for aluminum alloys [4]. This process may be applied on large surfaces by shifting the tool over a distance that is a fraction (called the overlapping ratio) of the modified region in the material [5, 6]. Fig. 1.2 presents the surface finish and stir zone (or nugget zone) shape of a 5083 aluminum alloy surface processed by FSP.

FSP is particularly well suited for low melting point metals, such as Al, Mg or even Cu alloys, since the tool can then easily be machined from hard steel. However, FSW, and thus possibly FSP, has also been applied to higher melting point metallic alloys such as steel and titanium making use of much harder at high temperature and wear resistant tools such as PCBN or W-Re [3].

FSP may be applied for the efficient manufacturing of metallic alloys based architectured materials. Indeed, the FSP tools allow locally modifying the microstructure of metal based alloys or assembling dissimilar materials. As largely discussed in the other chapters of this book, architectured materials often involve dissimilar material assemblies or gradients of properties that could be reached by the local modification of a bulk material. In addition, improving the mechanical performances of an entire structural component is usually not necessary. In practice, plasticity, damage and cracking is only initiated in regions presenting high stress concentration. A FSP treatment can thus be locally applied to these regions to make overall higher performance structural parts.

The present chapter will discuss the possible architectured materials that may be manufactured by friction stir processing. Most of the work that is presented here did not specifically aim at making architectured materials but some of the ideas can be exploited to make such new structural materials and definitely aim at improved overall performances by the smart combination of materials and processing. FSP may locally modify the microstructure of cast or wrought materials, process metal matrix composites (MMC), make sandwiches, foams or additively manufactured structures. The ability of making these modifications at the local scale make the nature of the material architectured. The aim is to process materials with improved lightweight performances, static or fatigue properties, crack resistance, toughness or wear resistance.

1.2 Local microstructure modifications and graded materials

1.2.1 Grain refinement

Friction stir processing is commonly known to produce a significant refinement of the grain size in the stir zone. This is due to the dynamic recrystallization process that takes place in the zone mixed by the tool shoulder and pin. The type of recrystallization mechanism likely depends on the processing parameters and material nature [7]. FSP may cause discontinuous [8] or continuous [9] dynamic recrystallization.

Fig. 1.3 shows the grain refinement observed in a twin-roll cast FSPed Al-Mg-Sc alloy [10]. In that particular case, the grain size is reduced by a factor close to 40. The effect of the rotational speed on the grain size is also evidenced in Fig. 1.3. A clear decrease of the grain size is observed as the rotational speed decreases [10, 11]. This is associated to a decrease of the maximum temperature as the rotational speed decreases due to less frictional and deformation heat generated by the process. Thus, grain growth is less activated after recrystallization. Other research teams have managed to further reduce the grain size in Al7075 [8,12,13] by hindering the grain growth by fast cooling

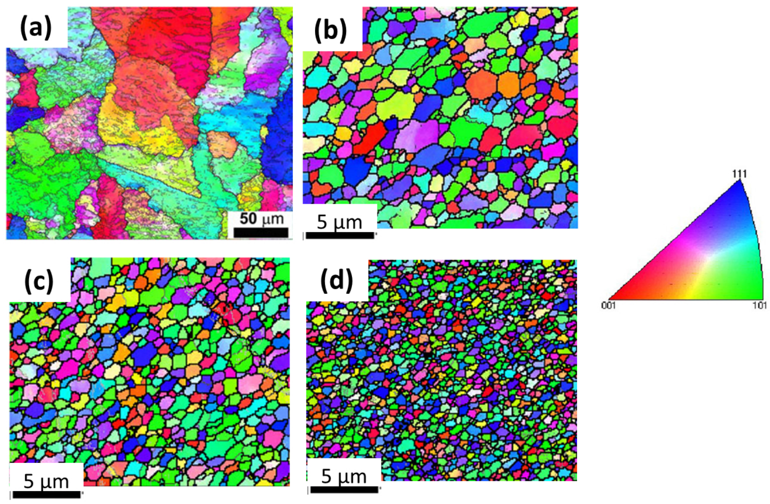

Fig. 1.3. Grain size and texture evolution due to FSP at various rotational speeds in a twin-roll cast Al-4Mg-0.8Sc-0.08Zr alloy (EBSD map). The advancing speed is kept constant at 3.4 mm/s. (a) Base cast material (mean size = 19 μm), (b) FSP at 800 rpm (mean size = 0.89 μm), (c) FSP at 400 rpm (mean size = 0.73 μm) and (d) FSP at 325rpm (mean size = 0.49 μm). From Kumar *et al.* [10].

using dry ice on the surface with an additionally cooled support anvil (100-400 nm [8], 25-40 nm [12]) or by liquid nitrogen circulating in the support anvil [13] (210-380 nm). Liquid nitrogen cooling of the FSP anvil may also refine grains in magnesium alloys, e.g. 300 nm in AZ61 [14] and 500 nm in AZ91 [15]. Dry ice surface cooling also allowed to refine the microstructure to a 50 nm mean grain size in pure Cu [16] near the exit hole. These grains then grew to a mean size of 300 nm in the final FSP stir zone, emphasizing the effect of the cooling stage on grain growth.

The grain refinement is not always homogeneous in the processed zone. Indeed, the grain size is generally larger on the top surface of the processed zone [8,17, 18]. This is associated to the extra heating due to the tool shoulder favoring grain growth after recrystallization. In the high entropy alloy Al0.1CoCrFeNi a graded increase of grain size is observed in the processed zone from the advancing (AS) to the retreating side (RS) [19]. This is due to both a difference of strain accumulation and a sluggish diffusion which controls and retards grain growth during cooling, entailing a hardness increase in the processed zone from the AS to the RS.

The importance of the pinning action of second phase particles on hindering grain growth and favoring particle stimulated nucleation during recrystallization has been particularly evidenced by Morishige *et al.* [20]. They have compared the grain size after FSP for pure aluminum presenting various degrees of impurities. They clearly show that smaller grains after FSP can only be maintained if second phase particles are present, i.e. in 99% purity Al compared to 99.999% purity Al. The alloying elements may also impact on the formation of extra barriers to the movement of dislocations like twins. Xue *et al.* [21] have evidenced more twin formation during FSP in copper containing 15%Al than in Cu-5%Al due to the lower stacking fault energy associated with the extra Al in solid solution. The grain size was similar in both alloys, i.e. 500-600 nm. The Cu-15%Al material presented significantly enhanced strength and ductility associated to the formation of these extra twin boundaries.

Thus, reaching ultra-fine grains or extra twin boundaries by FSP requires low maximum temperatures, fast cooling rates, second phase particles or alloying elements. During the FSP process, the strains are expected to be in the 5-10 range and the strain rates in the order of 10-400 s^{-1} [22]. FSP allows reaching locally, where needed, grain sizes that are typical of severe plastic deformation processes. Su *et al.* [8] reached a grain size and misorientation distribution typical of 10 ECAP (Equal Channel Angular Pressing) passes with a single pass FSP. Kulitskiy *et al.* [23] showed that FSPed Al-Mg-Sc presented only slightly larger grain size after 1 pass of FSP than after 12 ECAP passes (2.1 μm after FSP vs 1.2 μm after ECAP). More than 80% of high angle grain boundaries are found in an Al-Mg-Sc FSPed alloy [23, 24]. FSP can be easily performed locally contrarily to ECAP.

An issue related to the fine grains generated by FSP is that they are generally not very stable during a solution treatment above typically 450^{o}C in Al7010 [25] or above 490^{o}C in Al5083 [26]. Indeed, abnormal grain growth is likely to occur because the grains are free of dislocations or free of pinning phases at high temperature [25, 27]. Grains typically of a few millimeters have been reported [25, 27, 28]. Abnormal grain growth will inevitably lead to a loss in strength and ductility [29]. This may be problematic as sometimes a solution heat treatment[3] is necessary to fully dissolve the large precipitates prior to an aging treatment aiming at restoring the fine strengthening precipitation in aluminum alloys.

[3] The solution heat treatment is typically performed at temperatures larger than 500^{o}C in Al alloys.

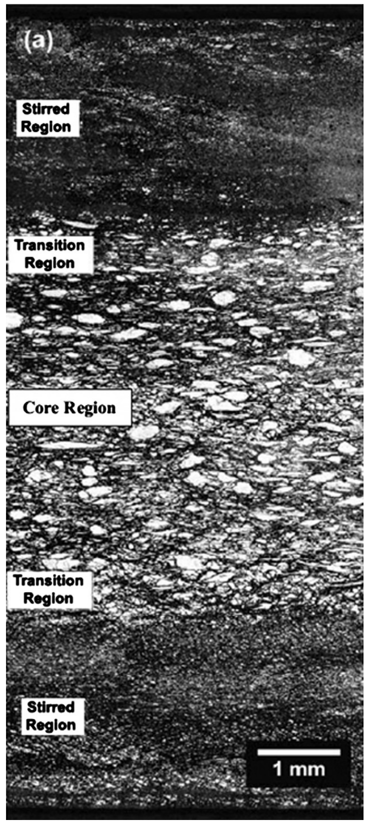

Fig. 1.4. Multilayered microstructure obtained by FSP a ZK60 magnesium alloy on top and bottom surface. From Mansoor *et al.* [33].

Many authors have evidenced increases in hardness and strength associated to the grain refinement by FSP in Al and Mg alloys [11, 14, 30–32]. The local modification of the mechanical properties is thus possible by the FSP process and associated grain refinement. However, not many authors have attempted to only partially process materials to take advantage of the possibility to make a multilayer. Mansoor *et al.* [33] have processed a ZK60 magnesium alloy on the top and bottom surface and report grains of 800 nm in the processed zone and a higher strength "multilayer" with only limited loss in ductility. Fig. 1.4 shows the multilayered structure they processed.

1.2.2 Cast materials: porosity elimination and microstructure homogenization

Cast materials have the particularity to contain porosities due to gas entrapping or gas dissolution in the molten state. Volume shrinkage associated to solidification is also a source of large porosities [34]. In addition, often the microstructure is inhomogeneous due to dendritic growth [34]. This may lead to low strength and premature failure. However, casting is an interesting process to manufacture geometrically complex parts. Thus, it may be interesting to be able to locally modify the microstructure of cast materials in order to improve the mechanical performances in regions of high stress concentrations where fatigue cracks are likely to initiate and propagate. Friction stir processing has largely proven to eliminate casting porosities and refine the microstructure [35–42]. This process may be applied locally and is thus an alternative to the hot isostatic pressing of the entire part [35]. Eutectic modifications are possible, e.g. by adding Sr in cast Al alloys [43] but are not likely to have a positive effect on casting porosities. The volume fraction of porosities might even be increased due to longer time spent at high temperature needed to ensure the eutectic modification [44].

Friction stir processing allows the elimination of casting porosities both in aluminum [35, 39, 41] and magnesium [39, 45] alloys. Ma *et al.* [36] have reported 0.1% of porosities in as-cast A356 and 0.02% when FSPed in the best conditions. Hannard *et al.* [28] have even reported the full elimination of porosities in wrought alloy 6056 after 3 passes of FSP. This is due to the large pressure under high temperature applied by the tool shoulder on the surface of the material. Prior porosities significantly decrease the ductility of cast materials [34] while many authors have reported a significant increase in ductility by FSP [36, 41, 46].

The cast microstructure is also homogenized and refined by FSP. Fig. 1.5 shows the breakage and homogenization by FSP of the inhomogeneous acicular distribution of Si rich particles in an Al-7Si-0.6Mg alloy [41]. The large plastic deformations of the FSP process cause the redistribution, fracture and erosion of coarse particles [3, 36] as will be further discussed for metal matrix composites (section 1.3). The aspect ratio of particles can be significantly reduced [36]. The homogenization is observed at a macroscopic scale through hardness measurements [35]. If performing overlapping passes, Ma *et al.* showed that the homogeneity of the hardness is maintained [37]. However, banded structure with coarse Si particles segregation have been reported for low rotational speeds [38]. A more homogenous and finer second phase distribution is generally observed at higher rotational speed [38,41]. Chen *et al.* [42]

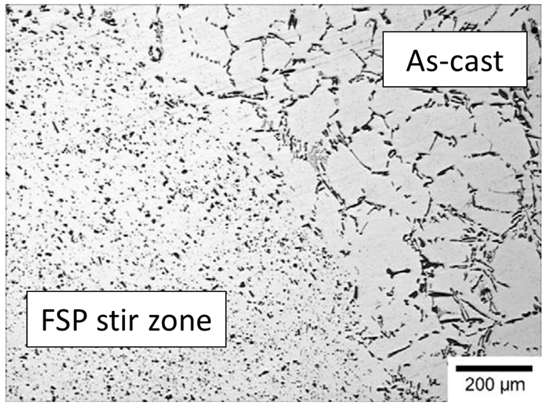

Fig. 1.5. Interface between the cast and FSP region in an Al-7Si-0.5Mg alloy (F357) showing extended microstructure refinement and homogenization in the stir zone. From Jana *et al.* [41].

have reported the alignment of the particles in the transition deformed region close to the stir zone (called the thermomechanically affected zone, TMAZ) in partially overlapping FSP leading to preferential failure at that location. In magnesium alloys, Feng *et al.* [40] show bands of higher content in $Mg_{17}Al_{12}$ particles in AZ80 alloy single pass FSPed material. In the double pass material this problem was solved. Hannard *et al.* [28] have quantified the microstructure homogenization due to FSP in Al6056. After one pass of FSP, the fragments of large particles are not yet homogeneously distributed, three passes are needed to ensure homogeneity.

In what concerns the mechanical properties, as already mentioned, the ductility of FSPed material is generally much higher than the ductility as cast [36, 41, 46]. In addition to porosity elimination, the redistribution and refinement of the second phases also significantly improves the strength and the ductility [41,47]. Jana *et al.* [41] have compared the fracture surface of as cast Al-7Si-0.6Mg (1.1% elongation at fracture) with the samples FSPed (20% elongation at fracture). The fracture surface presents a more ductile character with fine dimples in the FSPed samples while cleavage along the acicular second phases is observed on the fracture surface of the as-cast material.

The fatigue performances of FSPed cast materials are also impressively improved compared to their as-cast counterpart [45, 48–52]. This is mainly attributed to the elimination of porosities and to the particle refinement avoiding easy path for fatigue crack growth [48, 49, 52]. The fine second phase particles

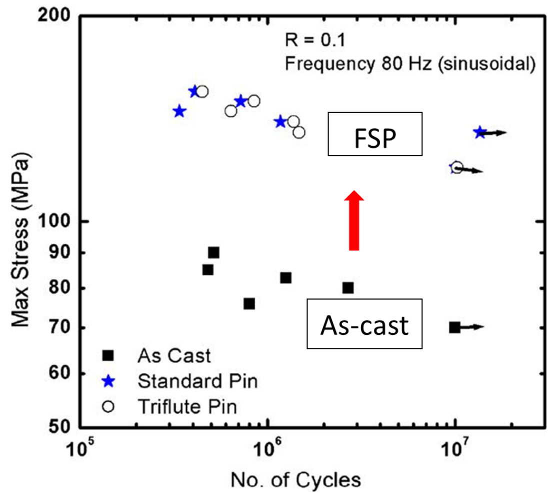

Fig. 1.6. Improved fatigue life of a A356 Al alloy by FSP under a stress ratio of R=0.1. Two tool pin geometries (standard and triflute) were tested showing no impact on fatigue life. Adapted from Sharma *et al.* [48].

distribution favors crack tip blunting by the ductile matrix [50]. Fig. 1.6 shows the increase by 80% of the fatigue stress threshold by FSP of an A356 cast Al alloy.

In what concerns fracture toughness, very limited results are available. Aktarer *et al.* [53] have measured the Charpy impact energy in as-cast and FSPed Al-12Si. It increased by a factor 7 from 1.2 J/cm^2 to 8.3 J/cm^2. Here again, acicular Si particles where found to be preferential path for fracture in as-cast Al-12Si leading to a facetted fracture surface, while a large amount of small dimples were found on the fracture surface of FSPed Charpy tested samples.

The wear resistance of FSPed cast materials may also be improved compared to their as-cast counterpart thanks to the finely distributed second-phase particles. A lower wear rate (typically divided by a factor 2) is found for FSPed A356 Al alloy compared to the as-cast A356 [54, 55]. The wear rate was found to decrease if the rotational speed is very large (1250 rpm) [54]. This is consistent with a better distribution and refinement of the second-phase particles at higher rotational speeds [38, 41].

1.2.3 Superplasticity

The superplastic potential at relatively low temperatures and high strain rates compared to other processing methods has been largely reported for both alu-

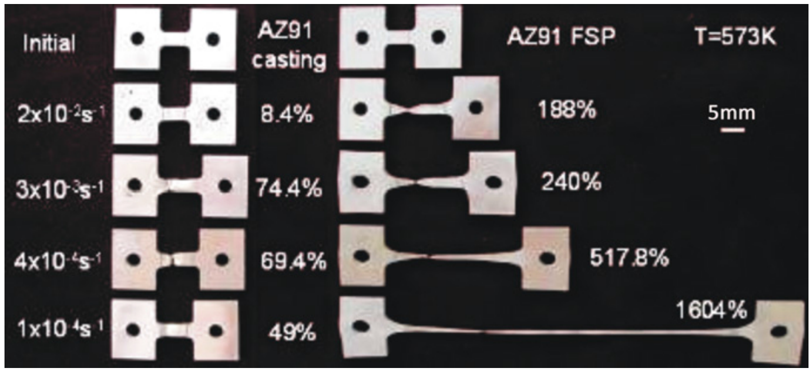

Fig. 1.7. Comparison of the superplastic behavior of as-cast and FSPed AZ91 magnesium alloy at various strain rates for a temperature of 573 K. From Zhang *et al.* [72].

minum [2,56–70] and magnesium [71–75] friction stir processed alloys. Fig. 1.7 shows the exceptional improvement of the plastic behavior of the FSPed AZ91 magnesium alloy compared to the as-cast material. High strain rate superplasticity allows to form sheets in a reasonable amount of time compared to materials presenting low strain rate superplasticity. Low strain rate superplasticity is rather classical for other severe plastic deformation processes but high strain rate superplasticity is exceptional. The main deformation mechanism leading to superplastic forming in FSPed materials is grain boundary sliding which is thus greatly enhanced in ultra-fine grain materials [56, 57, 61, 62, 70, 73] and in the presence of high angle grain boundaries [69] as typically found in FSPed materials. The appearance of the abnormal grain growth phenomenon is the upper temperature limit for superplastic forming [62, 65, 67, 68].

In the aim to process an architectured material with local ability for superplasticity, FSP could be applied locally. Mishra [59] reports the interest of making local FSP modifications to a part to ensure superplastic forming where needed, see Fig. 1.8.

1.2.4 Precipitation state and phase modifications

The high temperature reached during FSW and FSP generally affect the precipitation and phase distribution in metallic materials. Dissolution is enhanced in FSPed samples compared to just heated samples due to the shear driven effect [76]. Precipitate evolution may lead to gradients in mechanical properties that might be much more significant than what is resulting from grain refinement [77].

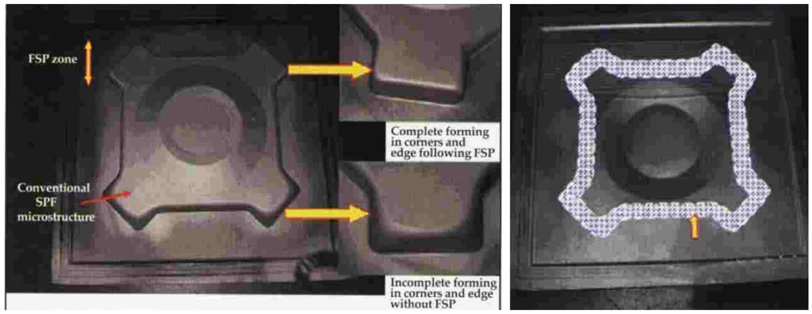

Fig. 1.8. Local modification by FSP of an Al7xxx alloy for superior superplastic formability. From Ref. [59], courtesy of M. Mahoney.

In aluminum alloys, the strengthening precipitates tend to dissolve in the stir zone leading to substantial softening [77–82]. Natural ageing may lead to the re-precipitation of GP zones that will slightly increase the hardness compared to a supersaturated state [82, 83]. The softening associated to the heating in the stir zone is also extended to the heat affected zones (HAZ). The HAZ generally present a lower strength than the stir zone due to the lack of dissolution of alloying elements in this zone that is rather subjected to precipitate coarsening [77,82]. Fig. 1.9 shows the gradient in hardness between the various zones of an Al6005A FSW in cold (advancing speed equal to 1000 mm/min) and hot (advancing speed equal to 200 mm/min) conditions. The hardness ranges from 65 HV to 105 HV. Fig. 1.9 also shows that a post-welding heat treatment may modify the hardness gradient enhancing the strength in the stir zone due to formation of fine strengthening precipitates (here β" precipitates). In thick FSPed Al alloys, the precipitate state may vary from the top to the bottom of the stir zone due to gradients in peak temperature [84,85]. This will lead to hardness gradient as shown in Fig. 1.10 for an Al2050 alloy. In cast Al-Si-Mg alloys, Mg_2Si precipitate dissolution in the stir zone has also been reported, and re-precipitation is possible during a post-welding aging treatment [36, 37].

In magnesium alloys, precipitate dissolution also occurs in the stir zone. For exemple, Xiao *et al.* [86] observed the dissolution of β-Mg(Gd,Y) in a FSP Mg-Gd-Y-Zr alloy. Jamili *et al.* [87] concluded that the $Mg_{24}Y_5Nd$ lamellar eutectic phase dissolves during FSP of WE43 alloy.

For details about the microstructure evolutions and resulting mechanical properties in high melting temperature materials, the reader is referred to Ref. [3].

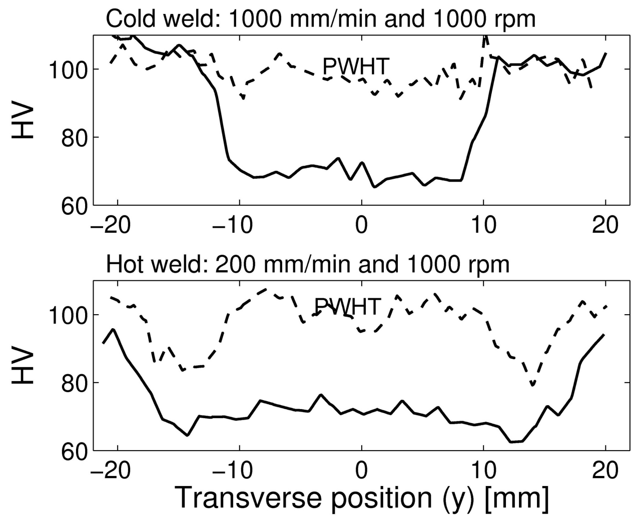

Fig. 1.9. Hardness gradient in the stir zone and heat affected zone of Al6005A-T6 friction stir weld performed in cold conditions at 1000 mm/min and 1000 rpm and in hot conditions at 200 mm/min and 1000 rpm. PWHT = Post-Welding Heat Treatment at 185^{o}C for 6h. From Simar *et al.* [81].

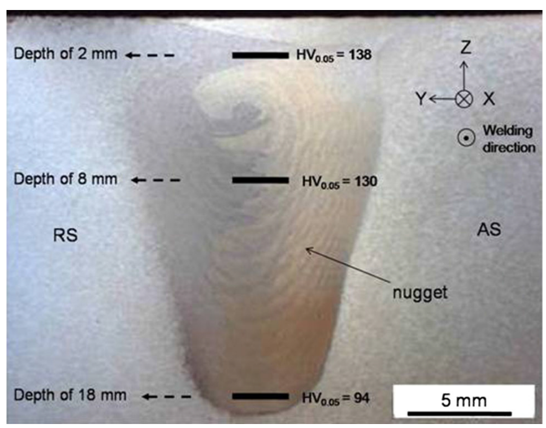

Fig. 1.10. Hardness gradient in the stir zone of thick Al2050 FS weld. From Avettand-Fènoël *et al.* [84].

The main limitation in processing these high melting point materials is the need for very hard tools, which might render FSP uneconomical for these materials. But, when cost is not part of the optimization criteria, FSP may also be considered for these materials. Seraj *et al.* [88] performed FSP on a AISI 52100 steel where the ferritic-pearlitic microstructure was transformed to a martensitic microstructure with retained austenite. This leads to a significant

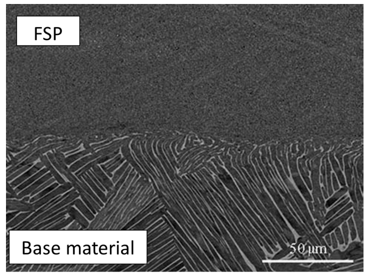

Fig. 1.11. Transition zone in a FSPed zone of a Ti6Al4V titanium alloy. From Pilchak *et al.* [89].

increase in hardness (by a factor 2) and a reduction of the wear rate (by a factor 15).

In Ti6Al4V titanium alloy, phase transformations are observed during FSP. Fig. 1.11 shows the modification of the microstructure between the base material and the stir zone in a cast Ti6Al4V alloy [89]. The base material presents α lamellae in prior β grains typically 1.5 mm in size while the recrystallized stir zone presents 1-2 μm size equiaxed α grains. Pilchak *et al.* [89] suggest that a FSP structure on the part surface could delay fatigue crack initiation while the core base material structure favors a lower fatigue crack growth. Thus, a multilayer material would present better fatigue performances [90]. Pilchak *et al.* [90] have shown an increase in fatigue life from 58,000 cycles in as-cast conditions to 300,000 cycles for some FSPed samples. In the work by Pilchak *et al.* [89], FSP was performed above the β transus. The FSP parameters were modified to perform FSP on a biphased $\alpha + \beta$ microstructure below the β transus [91] with a lower rotational speed and/or a larger advancing speed. In that case, regions of transformed β phase may be observed in-between equiaxed α grains [91]. Li *et al.* [92] have shown that faster cooling rates generated by higher advancing speeds lead to the formation of an α martensitic structure that is more wear resistant and may thus be interesting to generate on the surface of Ti6Al4V parts.

1.2.5 Texture modifications

In Al alloys the texture after FSP is usually close to random (see Fig. 1.3). The texture after FSP is not affected by the initial texture even when FSP severely deformed Al alloys [93].

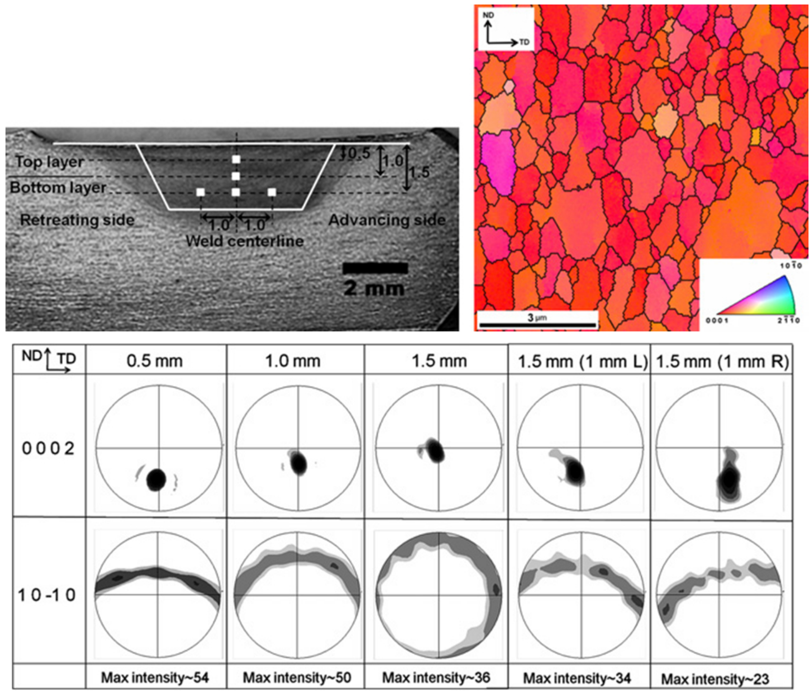

Fig. 1.12. Basal 0001 texture in a FSPed AZ31 magnesium alloy. The position in the stir zone significantly affects the texture orientation. From Yuan *et al.* [97].

In magnesium alloys, FSP clearly affects the texture [94–100]. Generally a strong basal texture is observed with an alignment of (0001) basal plane with the tool shoulder surface in the upper stir zone [95, 96, 99, 100]. Vargas *et al.* [100] have shown that this crystallographic texture is enhanced by a second pass of FSP in a ZKX50 alloy. Xin *et al.* [96] have shown that this basal texture evolves from the processing direction to the transverse direction respectively from the center of the stir zone to its periphery. Yuan *et al.* [97] have shown that the tilt of the basal plane depends on the depth. The angle between the basal plane and the normal direction of the plate surface varies from 37 at 0.5 mm depth to 86 at 1.5 mm depth, see Fig. 1.12. The strong texture impacts the anisotropy of plasticity in the FSPed samples with significantly higher ductility in the transverse direction compared to the processing direction and harder (respectively softer) material than the base material in the transverse direction (respectively in the processing direction) [97].

1.3 Metal Matrix Composites (MMC) and graded materials

Friction stir processing is also used to process metal matrix composites (MMCs) and graded materials. The reader interested by the FSW of metal matrix composites can also refer to the review by Avettand-Fènoël and Simar [101]. Indeed, FSW of MMC presents some common features with the use of FSP to make these materials.

The architectured materials presented in section 1.2 generally refer to an evolution of the microstructure in the bulk or at the surface of the materials, affecting in particular the grain size. In the case of MMCs, and as previously mentionned in section 1.2.1, the grain boundaries pinning by second phases can enhance the grain refinement effect of dynamic recrystallization. This is for instance shown in a FSPed Al_2O_3 reinforced ferritic stainless steel [102], in a FSPed TiC reinforced ferritic steel [103] or in a FSPed Al_2O_3 reinforced pure titanium, particularly if the latter reinforcements are very small, i.e. 20 nm vs 80 nm [104].

1.3.1 Practical concerns for the elaboration of MMCs and graded materials

Various possibilities as well as disposals of reinforcements are reported in literature to develop MMCs or graded materials by FSP (Fig. 1.13). Reinforcements may be powders, fibers or even nanotubes.

Disposals with powders or nanotubes - Grooves can be machined at the surface of the workpiece and then filled with powder particles or nanotubes (Fig. 1.13(a)). The assembly is then sealed either with a pinless tool [102,105–107] or covered with a thin sheet [5,108] to avoid powder ejection and loss during FSP. Other authors drilled some periodic holes (powder reservoir) at the surface of the workpiece along its depth and subsequently filled them with powder particles (Fig. 1.13(b)) [109,110]. Other methods consist in machining blind-grooves or blind-holes under the workpiece surface (Fig. 1.13(c)) [109]. As schematized in Fig. 1.13(d), powder particles can also be mixed in a volatile medium, such as ethanol, methanol, lacquer or glue in spray, and deposited on the surface of the workpiece [106]. A pinless tool is then used to incorporate the powders near the workpiece surface. FSP is performed subsequently with a classical tool [106]. Alternatively, a coating can be deposited on the surface of the workpiece by a surface treatment such as plasma spraying. The coated plate is then friction stir processed for incorporation near the surface (Fig. 1.13(e)) [111]. A consumable composite FSP tool can also be used to directly insert powder particles in the substrate (Fig. 1.13(f)) [105,106,112].

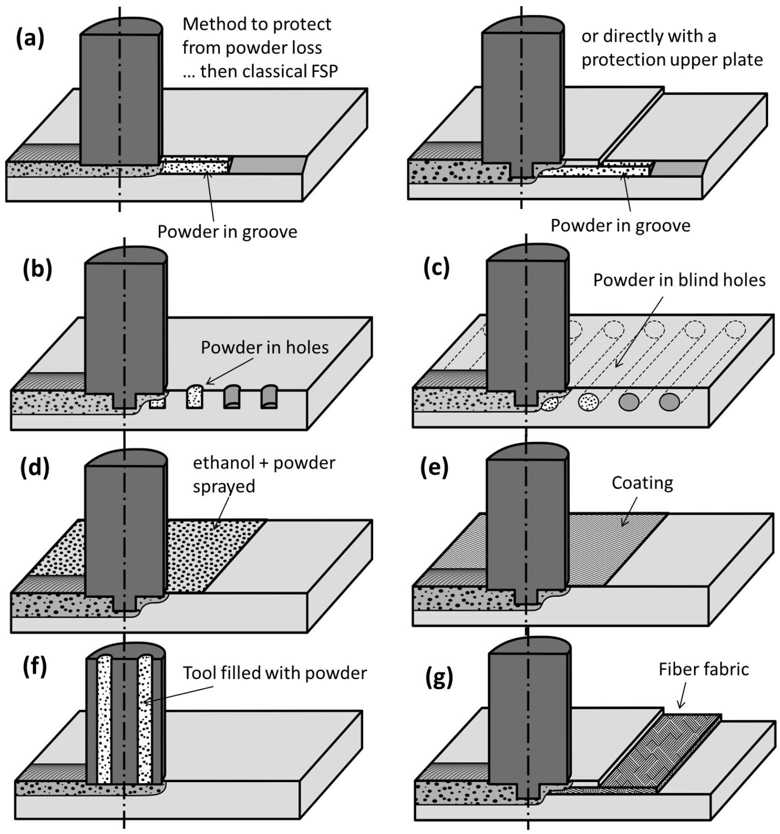

Fig. 1.13. Schematic of various reinforcement disposal methods: (a) powder placed in grooves machined near the surface; (b) powder placed in holes drilled near the surface; (c) powder placed in blind holes; (d) powder dispersed in ethanol and sprayed on the surface; (e) coating prior to FSP; (f) consumable composite pinless tool; (g) fabric stacked between two plates (Schematic by N. Jimenez-Mena).

Disposals with fibers - Concerning the setting to introduce short fibers in a metallic matrix, a fabric can be stacked between two metallic plates. FSP on the lap assembly will break the fibers of the fabric and distribute short fibers in the processed zone (Fig. 1.13(g)). Mertens *et al.* [113] have applied this process to reinforce Mg alloys with carbon fibers.

Disposals with strips - Liu *et al.* [114] directly placed a strip of an amorphous alloy in a groove machined at the surface of the Al alloy workpiece.

Disposal with gas - In this method, the first FSP pass is performed under reactive nitrogen blown in front of the advancing tool in order to introduce nitrogen gas into the stir zone of a workpiece machined with a groove. This was, for example, applied to develop in-situ TiN reinforced Ti. A TiN quasi uniform distribution was obtained after three subsequent FSP passes under argon [115].

The disposal methods relying on the insertion of powder in grooves or holes (Fig. 1.13(a) to (c)) are limited to very specific applications and are difficult to extend to large series. Placing ethanol mixed with powder on the surface is certainly an interesting method but it sounds difficult to ensure the homogenous distribution of the particles in the MMC (Fig. 1.13(d)). The use of a consumable pinless tool (Fig. 1.13(f)), which is in some points of view similar to additive manufacturing, leads to a multilayered MMC coating which is quite rough. Furthermore, the manufacture of the consumable pinless tool seems ticklish to transpose at the industrial scale. The use of coatings mixed by FSP (Fig. 1.13(e)) or the fiber fabric method (Fig. 1.13(g)) are more industrially efficient methods that have the potential to lead to a homogenous distribution of the fibers.

1.3.2 Potentiality and flexibility of the process

FSP is particularly interesting to develop architectured materials involving MMCs. Indeed, FSP leads to a better bonding between the matrix and the reinforcements compared to other processes involving casting [116–118]. Besides, this environmentally-friendly surface treatment process is flexible and offers many possibilities related to the volume of the treated zone, the nature of the systems of materials and the formation of in-situ MMCs.

Volume and extension of the processed zone

FSP is attractive as it offers the possibility to develop surface composites as well as functionally graded composites [6]. It is indeed flexible since a pinless tool may treat only the extreme surface of the workpiece, or a tool with variable pin lengths or retractable pins may architecture the microstructure with differences from the top to the bottom of the plate [6]. In addition, the width of the processed zone can be adapted in order to tailor the volume fraction of reinforcement in the MMC. This is done by using a suitable setting of process parameters. For instance, the volume of the processed zone can be increased using a low advancing speed [113] or a large rotational speed [106]. Indeed, such processing conditions contribute to an enhancement of the malleability of the base material workpiece due to a higher processing temperature. An increase of both the pin and the shoulder diameters as well as a reduction of the rotational speed with increasing number of overlapping passes can also enable to adjust the size of the processed zone. This method was tested during FSP of Al5059 with 50 vol.% carbon nanotubes [119]. The use of a tool design with three pins under the shoulder [120] and of successive passes partially overlapping [5] are other ways to extend the width of the processed zone. FSP assisted by a supplementary electrical heat input was further shown to enlarge the processed zone size [106].

The powder disposal method (grooves, holes, etc) also affects the local volume fraction of reinforcements [109]. For instance, according to the size (width or depth) of the machined grooves [104, 121] or according to the number and the size of the holes drilled in the workpiece [109], the volume fraction of reinforcements packed into them and finally dispersed in the MMC changes. In order to increase the volume fraction of reinforcements in the composite, it is also possible to machine new grooves at the surface of the workpiece following a first FSP treatment. These new grooves are then filled with powders before new FSP passes [122]. However, this last technique sounds labor intensive but is effective in increasing the volume fraction of reinforcements.

Variety of systems

On the point of view of the nature of matrix/reinforcement couples, various systems have been tested by FSP as detailed in Table 1.1. In the case of in-situ MMCs elaborated during FSP by the introduction of elementary components, intermetallic compounds were formed during the process and play the role of reinforcements. As mentioned previously, the initial reinforcements can further present various shapes namely particles [5], which can be coated to improve their bonding with the matrix [132], strips [114], coatings [144], fiber fabrics [113] or nanotubes [107, 119, 131, 151]. As one may see, the variety of couple reinforcement/metallic matrix is very large and allows considering any system that may lead to enhanced performances that may be mechanical or functional as will be discussed in section 1.3.4.

The initial reinforcement can have micrometric or nanometric sizes. However, getting a uniform distribution of nanosized particles is difficult. Asadi *et al.* [118] noted an agglomeration of nanometric Al_2O_3 in Mg based composite because of the bad wetting between the reinforcements and the matrix, but obtained a uniform distribution of the micrometric Al_2O_3. Similarly, nanoparticles of TiC in mild steel were heterogeneously distributed after one pass of FSP because of their high cohesive energy [103]. By comparison, in the case of

Table 1.1. Nature of matrix and reinforcements of MMC systems processed by FSP. IMC = Intermetallic compounds.

	Systems	Relevant references
Base materials	Al based	[6, 105, 108, 110–112, 114, 116, 119, 123–143]
	Cu based	[5, 121, 122, 145–149]
	Mg based	[107, 113, 117, 118, 150–157]
	Ti based	[104, 109, 115, 156, 158]
	Steel based	[102, 103]
	Bronze	[159]
Amorphous reinforcements	SiO_2	[133, 150, 153]
	$Al_{84.2}Ni_{10}La_{2.1}$	[114]
Metallic reinforcements	Ni	[128, 130, 154]
	Mo	[127]
	Fe	[134]
	Cu	[144]
	Stainless steel	[136]
	W	[139, 160]
Ceramic reinforcements	AlN	[148]
	Hydroxyapatite	[156]
	SiC	[6, 102, 105, 112, 117, 118, 123, 132, 135, 145–147, 149, 158]
	TiC	[103, 109, 147]
	B_4C	[121, 129, 147]
	Al_2O_3	[102, 104, 105, 116, 118, 147, 152]
	Y_2O_3	[5]
	TiO_2	[142, 143]
	TiN	[115]
	TiB_2	[116]
	ZrB_2	[141]
	WC	[147]
	SiO_2	[137, 155]
	ZrO_2	[157]
	Cr_2O_3	[111]
IMCs	NiTi	[110, 124, 140]
	Al_2Cu	[126]
	Al_3Ti	[126]
Other	Graphite	[122, 161]
	Carbon	[107, 113, 119, 131, 151]
Hybrid reinforcements	$SiC + MoS_2$	[125, 144]
	$SiC + Al_2O_3$	[108]
	Al_2O_3 + C nanotubes	[161]
	$Al_2O_3 + TiB_2$	[138]
In-situ made reinforcements	$Al_{12}Mo + Al_5Mo$	[127]
	$Al_{13}Cr_2$ (4 passes)	[111]
	$Al_{11}Cr_2$ (6 passes)	[111]
	Al_3Ni	[130]
	Al_3Ni_2, Mg_2Ni, AlNi, $MgNi_2$	[154]

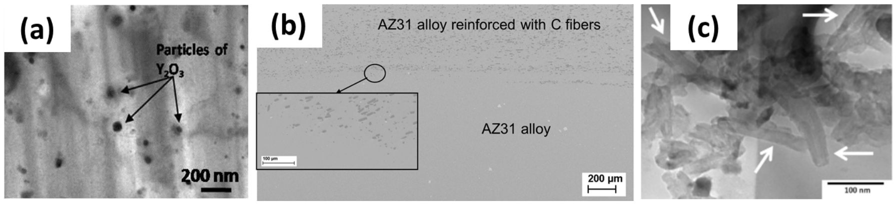

Fig. 1.14. (a) Cu reinforced with Y_2O_3 particles (from Avettand-Fènoël *et al.* [5]). (b) AZ31 Mg alloy reinforced with C fibers (for research project, see Mertens *et al.* [113]). (c)- Al 5059 reinforced with C nanotubes (indicated by white arrows) after 2 FSP passes (from Izadi *et al.* [119]).

Mg based composite reinforced with micrometric SiC, although SiC particles do not agglomerate, the good wetting between Mg and SiC reinforcement leads to a heterogeneous distribution of SiC particles [118]. Moreover, at another size scale, Bauri *et al.* [128] proved that with an initial powder particle size of 70 μm of Ni, FSP does not lead to a uniform distribution of Ni reinforcements in the Al matrix whereas their distribution becomes uniform during FSP of 10 μm sized particles. In the same way, during FSP of AA5083 Al alloy with SiC particles of 119 or 37 or 12 μm mean size, the smallest sized reinforcements lead to higher concentration along the bead surface and to a smooth gradient in volume fraction both in depth and along the transverse direction [6]. Some examples of different MMCs obtained from various reinforcements shapes are displayed in Fig. 1.14.

Ex-situ or in-situ MMCs and graded materials

Ex-situ or in-situ MMCs may be processed by FSP. Ex-situ composites contain reinforcements produced separately and then introduced in the matrix. In-situ composites contain reinforcements produced during the process. In-situ composites may be formed via:

- a phase transformation like crystallization of an amorphous reinforcement [114];
- a chemical reaction between the matrix and initial solid elements inserted within it [111, 126, 127, 130, 133, 134, 137, 144, 154, 162], e.g. Al + $SiO_2 \rightarrow$ Al/Al_2O_3+SiO_2 [133];
- a reaction between the matrix and the reactive gas, such as nitrogen, flowing in the zone treated by the FSP tool [115].

The reinforcements produced in situ via chemical reactions are very fine (for instance about 100nm [111]), thermodynamically stable and generally uniformly distributed in the matrix [126]. Besides, they present a good interface with the matrix.

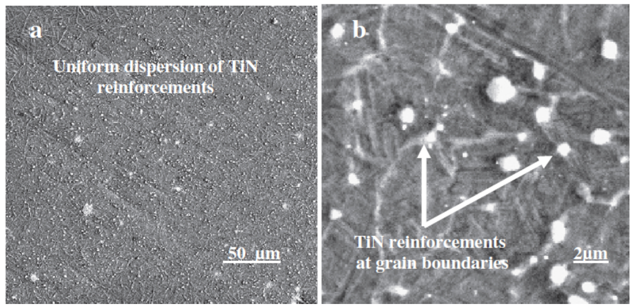

Fig. 1.15. TiN/Ti MMC processed in situ by FSP (from Shamsipur *et al.* [115]).

Some undesirable or unexpected chemical reactions or phase transformations can also occur during FSP due to the presence of the reinforcements. This may have the positive effect of further increasing the reinforcement effect. During FSP of Mg with SiO_2 particles [153], the good affinity between Mg and Si leads to the formation of additional Mg_2Si reinforcements in the Mg composite. These Mg_2Si are in complement to the amorphous initial SiO_2 particles still maintained after FSP. In the case of FSP of a ferritic stainless steel with SiC particles [102], SiC reacted with the matrix to form Cr_3Si and $(Cr,Fe)_3C_7$ precipitates and further induces the matrix phase transformation into Fe_3Si IMC and solid solutions of Si and C in a ferritic matrix. During FSP of CP-Ti under nitrogen, the formation of in-situ TiN precipitates (see Fig. 1.15) occurs together with the martensitic phase transformation of α-Ti matrix because of the formation of an N interstitial solid solution in Ti [115].

1.3.3 Effect of process parameters on the architectured microstructure of the MMCs and graded materials

Various process parameters, which directly govern the material flow during the process, can have an effect on the architecture of the MMCs and the graded materials. The homogeneity of reinforcement distribution and their structural stability may be affected. Both will directly govern the properties of MMCs. The following will discuss the effect of the groove location on the workpiece, the number of passes, the rotational and advancing speeds, the change of the tool direction sense at each new pass, the heat input and the tool geometry.

Groove location and size - Gandra *et al.* [6] showed that a good dispersion of reinforcements is ensured provided the groove machined at the surface of the workpiece is located in the pin flow zone, i.e. in the core of the stir zone, and not in the shoulder flow zone, i.e. near the top surface. In addition, a reduction of the groove width leads to a better distribution of reinforcements [147].

Number of passes - Several passes are generally required to disperse the reinforcements, in particular if they are nanometric [155]. An increase of the number of passes was indeed shown to reduce the clustering of powdered reinforcements [155, 158] and to improve their fineness and homogenize their distribution [103, 116, 118, 129, 130, 146, 152–155, 158, 162]. X-ray tomography analyses showed that fiber reinforcements follow the material flow induced during each pass [113]. One may thus question the uniform and random distribution of such reinforcements which present directionality by opposition to the particle reinforcements.

Besides, by increasing the number of passes, the porosity at the matrix-reinforcement interface is reduced and the interfacial bonding is enhanced. For example, after one FSP pass, some porosities are observed at the SiC/Cu interfaces of the MMC but are not observed after 2 passes [145, 149]. Thus FSP improves the densification of the MMC as shown by Khayyamin [155] and already presented in section 1.2.2 for cast alloys.

The multiplication of passes may however also entail a structural instability of reinforcements and a change of their morphology by fracture and blunting. For instance, Bauri *et al.* [128] evidenced a fracture of initial Ni 70 μm sized powder particles during FSP of Al based MMC. Li *et al.* [109] also noticed a refinement during FSP of initial 5 μm sized TiC introduced in Ti-6Al-4V alloy reaching the nanometric scale. A refinement of hydroxyapatite particles introduced in Mg was also observed during FSP due to their breaking. Their morphology changed from flaked to spherical [156]. Izadi *et al.* [119] observed the fracture of some carbon nanotubes, then their disappearance which leads to spherical shelled carbon structures and formation of Al_4C_3. Three passes were required to homogenize the dispersion of reinforcements at the expense of the maintenance of the nanotubes shape. Mertens *et al.* [113] detected an erosion of carbon fibers in Mg based MMC obtained by FSP. Abdollahi *et al.* [154] showed an evolution of the nature of the reinforcements produced in situ according to the FSP passes number, namely a transformation of Al_3Ni_2 + Mg_2Ni formed in situ after the first FSP pass of AZ31 with Ni powder, into AlNi+$MgNi_2$ after subsequent passes.

Change of the direction of the tool advance at each new pass - The asymmetric feature of the FSP process due to a difference of material flow on advancing (AS) and retreating (RS) sides leads to the agglomeration of reinforcements on the AS [146]. Some authors changed the direction of the tool advance at each new overlap pass to get an homogeneous distribution and a similar density of reinforcements on AS and RS [108, 152, 153].

Rotational and advancing speeds - Like the increase of the number of passes, a greater rotational speed [116, 147, 152, 162] or a reduction of the advancing speed [116, 145, 147, 151] leads to a refined distribution of reinforcements. Indeed, they contribute to an enhancement of the malleability of the base material workpiece and thus improve the stirring effect [106]. As a consequence, since the processed zone is expected to be larger, the volume fraction of reinforcements is reduced [113]. Nevertheless, a significant increase of the rotational speed may lead to the tool fracture [158].

Friction stir vibration processing - In friction stir vibration processing, a normal vibration is applied to the processed line during the process while SiO_2 particles are incorporated in an Al alloy [137]. Vibrations decrease the grain size in the processed zone, improve the homogeneity of the distribution of reinforcements by contributing to the breaking up of agglomerated particles. This finally leads to enhanced hardness, strength and ductility [137].

Supplementary heat input - The use of an electrical current which passes through the shoulder into the substrate can thermally assist the FSP by improving the substrate viscoplasticity [106, 140]. This increases the volume of the processed zone although it reduces the volume fraction of reinforcements within it. It then promotes the homogeneousness of the reinforcements dispersion and avoids the formation of clusters. This alternative which may easily be industrialized could avoid to increase the number of passes to get a suitable, uniform and fine distribution of reinforcements in the MMCs [106].

Tool wear - FSP tools are generally made of hard steels like H13 steel for light alloys (with eventually a surface nitriding and oxidizing treatments [106]). WC/Co, PCBN, InRe, WRe, Co alloys and WC are preferred for processing MMCs and graded materials [144]. These tools are however expensive and their major concern is their wear which increases with both the abrasive feature and the volume fraction of the reinforcements [105]. The dimensions of a WC tool are for instance reduced by more than 20% during FSP of a mild steel with nanosized TiC reinforcements after four passes, which leads to the insertion of WC tool debris in the MMC processed zone [103]. It is worth noting that similar concerns, occur during friction stir welding of MMCs [101]. Various solutions were consequently proposed to reduce the tool wear during FSW. The process could be assisted by an electrical current in order to improve the stirring and to favor the viscoplasticity of the base material surface [106]. Besides, although some authors improved the reinforcement distribution with a threaded pin [152], an unthreaded pin is generally recommended to reduce tool wear otherwise the threads are abraded by the reinforcements during the process [163–165].

Tool geometry - The pin shape is an important factor since it governs the material flow and thus the quality of the reinforcements distribution [122]. The ideal pin would be square shaped, which entails a pulsating action leading to a uniform distribution of the reinforcements [166, 167] or a smooth frustum like tool shape which promotes a uniform material flow [163]. The use of three-fluted tool shape during FSP of Al_2O_3 reinforced Mg MMCs indeed led to cavities and microvoids [152]. Another study concerned by FSP of Cu with graphite particles showed that a triangular pin leads to a larger processed zone, to a better dispersion of the reinforcements than other tool shapes [122].

1.3.4 Mechanical and functional properties of FSP MMCs and graded materials

The use of several passes and of a judicious and suitable setting of process parameters was shown to improve the dispersion of the reinforcements (Fig. 1.13) and thus are expected to enhance the surface and bulk properties.

Surface composites

Hardness - Like in most MMCs, the hardness of the MMC is generally larger than its matrix [111, 112, 115]. Shamsipur *et al.* [115] processed a TiN/Ti surface composite by FSP. Particles were embedded 6 mm deep[4] in a commercially pure Ti workpiece machined with a 3 mm deep groove subjected to reactive nitrogen. The surface composite reinforced with only 2.3 vol.% TiN (Fig. 1.15) presents a promising 972 HV hardness which is about 6 times larger than that of the commercially pure Ti (Fig. 1.16). Comparing reinforcement size effects, the hardness of the processed zone of Al_2O_3 reinforced Ti based MMC with a 20 nm size of reinforcements is larger than when they are 80 nm in size [104].

[4] The latter surface composite is significantly deeper than those obtained by classical diffusion or remelting nitriding methods.

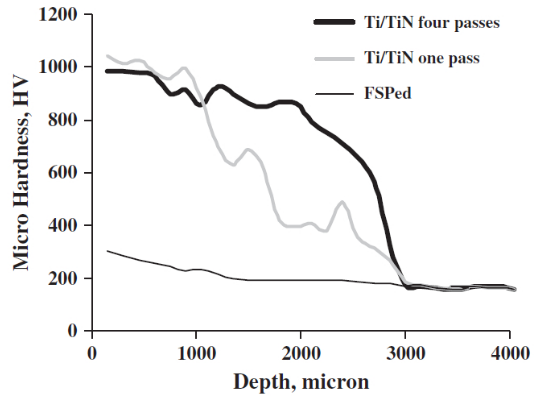

Fig. 1.16. Hardness of the TiN/Ti MMC processed in-situ by FSP (from Shamsipur *et al.* [115]).

Ductility - Compared to the TiC reinforcements, the stainless steel reinforcements in Al lead to a better ductility of the metal matrix composite due to the deformable nature of stainless steel and low Al work hardening around the reinforcements [136]. Besides, an increase of the number of passes from 1 to 5 was shown to increase the elongation from 12.5% to 24.5% for the W reinforced Al based composite [160].

Wear resistance - Many surface composites processed by FSP aim at improving wear resistance [103, 112, 118, 122, 129, 149]. Barmouz *et al.* [149] obtained a better wear resistance (Table 1.2), mechanical resistance and lower ductility by reinforcing Cu with 30 nm than with 5 μm sized SiC particles by FSP. Sarmadi *et al.* [122] showed that a 22 vol.% graphite reinforced Cu based MMC developed by 4 passes of FSP presents a friction coefficient 79% lower and a resistance to wear 65% greater than the pure annealed Cu because of the lubricating property of graphite. The TiC reinforced mild steel FSPed surface nanocomposite presents a wear resistance against steel disk two to three times greater than that of the steel substrate [103]. This behavior is attributed to a lower coefficient of friction and a greater hardness value of the surface composite. These are favored by a fine distribution of nanosized TiC and the refinement of the grain size.

The surface MMCs with both a hard and a soft kind of reinforcements are generally known to improve the wear resistance compared to their counterpart with a single kind of reinforcement [144]. The self-lubricating property and the wear resistance of surface of hybrid SiC + MoS_2 / Al5083 MMC was for instance higher than for SiC (or MoS_2)/ Al5083 MMC [125]. Another example deals with the 0.1% Al_2O_3 + 0.2% carbon nanotubes AZ31 MMC which presents a better wear resistance and a lower friction coefficient compared to the MMCs with one single kind of reinforcement or compared to the base material [107]. Concerning the wear resistance of a FSPed SiC-Al_2O_3/1050-H24 Al based MMC, the volume wear loss depends of course on the applied load during the test but also on the SiC/Al_2O_3 ratio. For a 5 N applied load, the hybrid MMC with 80% SiC and 20% Al_2O_3 presents a wear resistance greater than their counterparts with a single kind of reinforcement. For 10 N applied load, the wear resistance does not depend on the kind of reinforcement and is very close to that of the FSPed base material [108].

Corrosion - An addition of hydroxyapatite (HA) to Mg by FSP would weaken the basal texture of Mg thereby deteriorating the corrosion resistance to less than 20% of that in FSPed Mg. In the composite, the protective mixed layer was more easily generated on the surface since HA particles can act as nucleation sites. Although the accumulation of corrosion products is high, these products are porous and cannot prevent corrosion efficiently [156]. The 5A06 Al alloy based MMC with initial amorphous Al84.2Ni10La2.1 reinforcement was shown to present a lower corrosion density, a higher passivation current than the base material and a passivation zone [114].

Optical properties - Gudla *et al.* [142, 143] studied the optical properties of an aluminum alloy containing finely distributed TiO_2 particles after surface anodization. The color of the TiO_2 containing sample was much lighter. The reflectance of the surface is decreased as the anodizing time increases due to TiO_2 degradation.

Table 1.2. Dry wear rate in pure Cu and in FSPed samples (data from Barmouz *et al.* [149])

Sample	Wear rate (mm^3/Nm)
Pure Cu	$9.366\ 10^{-5}$
FSPed Cu - 6vol%SiC (5 μm)	$8.107\ 10^{-5}$
FSPed Cu - 18vol%SiC (5 μm)	$7.293\ 10^{-5}$
FSPed Cu - 6vol%SiC (30 nm)	$5.950\ 10^{-5}$
FSPed Cu - 18vol%SiC (30 nm)	$3.931\ 10^{-5}$

Graded bulk MMCs

Thermal properties - The shape memory of the NiTi reinforcements decrease the coefficient of thermal expansion of the Al alloy in the 10 vol.% NiTi 6061 Al MMC which leads to a good combination of adjustable damping and thermal physical properties through a proper heat-treatment process [124].

Electrical properties - The FSP of a billet of carbon nanotubes (CNT) reinforced AA6061 MMC previously obtained by powder metallurgy leads to a slight increase of its electrical conductivity because of the Mg and Si segregation at the CNT/Al interface after heat treatment which led to the formation of precipitates free zones near the CNTs. This increase in electrical conductivity to a lower extent may also be attributed to the random distribution of the nanotubes in the matrix due to FSP [131]. Oppositely, the addition of SiC particles to Cu by FSP led to an enhancement of the electrical resistivity of pure Cu. But the electrical resistivity of the MMC did not evolve significantly with an increase of the number of passes [168]. The same observation was reported in the case of Al based composite reinforced with W particles [160].

1.4 Lap welding metallic sandwiches

Friction stir welding and processing allow assembling dissimilar materials in an easy way in butt or lap welding configurations [3]. In the present chapter, the main issues related to the dissimilar metal lap welding by FSW will be discussed. Indeed, if one wishes to process architectured metal sandwiches, FSP might be an interesting option, see Fig. 1.17. FSP will ensure reconstitution of the metallic continuity at the interface between the two metals.

Sandwich-like architectured materials may be processed using friction stir lap welding. The interested reader is referred to the review on FSW of dissimilar metals by Simar and Avettand-Fènoël [169]. These structures could be processed in order to improve surface properties or combine efficiently properties of different materials. For example, the wear resistance of soft and ductile materials could be improved by placing a hard material sheet on top. The corrosion resistance may also be improved with a cover sheet, e.g. steel plates covered with Al or stainless steel sheets, or magnesium plates covered with Al. Li *et al.* [170] have processed an Al/Ti-6Al-4V bi-layer by friction stir lap welding, see Fig. 1.18. They claim that these assemblies may present interest for the good combination of high specific strength titanium alloy with high

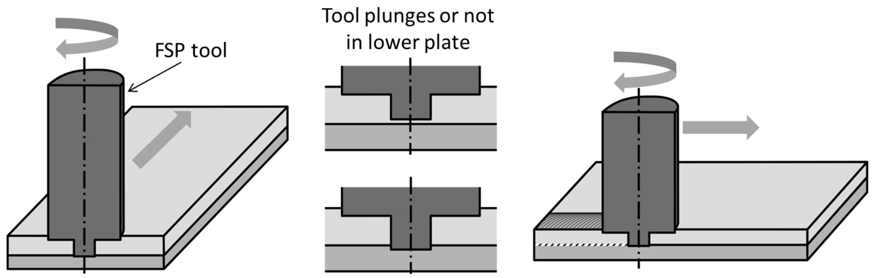

Fig. 1.17. Schematic of the lap FSP on a sandwich of metal plates (Schematic by N. Jimenez-Mena).

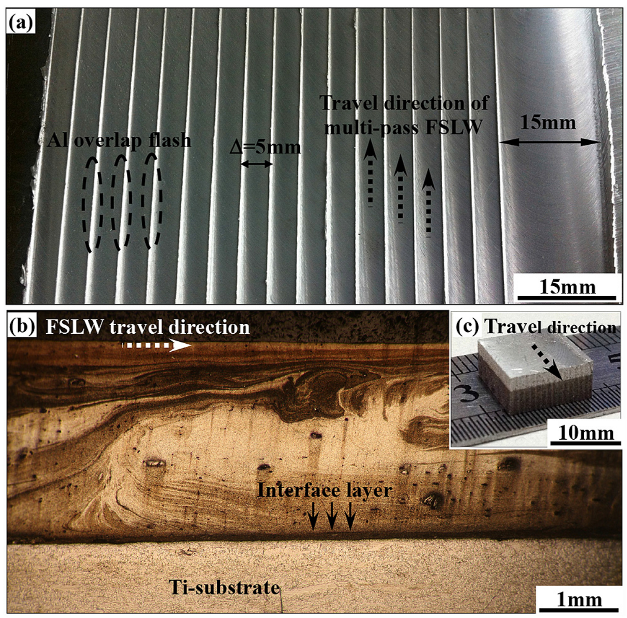

Fig. 1.18. Multipass friction stir lap welding to process an Al/Ti-6Al-4V bi-layer (from Li *et al.* [170]).

thermal conductivity aluminum alloy. Liu *et al.* [171] processed an Al-Si laser cladded coating by FSP and reached better corrosion resistance compared to the non-FSPed samples due to the suppression of coating cracks and pores. Finally, another interest of this type of assembly might be the processing of complex and brittle intermetallic phases already in the right shape and composition. The formation of the final material is ensured by a diffusion thermal treatment [172].

Dissimilar metal FS welding leads to the formation of intermetallic compounds at the interface. For example, Fe_2Al_5, Fe_4Al_{13}, $FeAl_3$ and FeAl intermetallic compounds have been reported in aluminum to steel lap welds [173–176]. $TiAl_3$ is systematically reported in aluminum to titanium welds [177] as well as magnesium alloys containing aluminum to titanium welds [178]. In the Al-Cu dissimilar FS welds many intermetallic compounds can be formed but Al_2Cu and Al_4Cu_9 are systematically reported [179]. These intermetallics are generally brittle leading to premature failure compared to the base materials [176].

In dissimilar metal friction stir lap welding, the softest material is generally placed on top and is in contact with the tool shoulder. For example, in a stack of aluminum and steel plates, aluminum will be placed on top of the steel plate [174]. Indeed, this configuration leads to lower tool wear. It is even possible to avoid plunging the tool pin inside the lower harder plate and ensure the welding by heat conduction near the interface [180], see Fig. 1.17. However, this does not always lead to sufficiently good mechanical properties [180]. Therefore, Haghshenas *et al.* [176] have proposed to place a low melting point interlayer to promote reactivity, e.g. Zn or Al-Si coating between an aluminum and a steel plate. Zn coated steel has also been used in this perspective [174, 181]. Zhang *et al.* [182] have even fully suppressed the tool pin and placed a Zn sheet between an Al and steel plate. The melting of the Zn sheet leads to an excellent planar joint presenting a good strength at medium advancing speeds. Another option is to place the steel plate on top and use a WC tool to heat the steel plate and ensure the local melting of the bottom aluminum plate at the interface [183, 184], see Fig. 1.19(a). The process is called Friction Melt Bonding (FMB). Fig. 1.19(b) presents the resulting interfacial microstructure of this new process. The advantage of these solutions in what concerns architectured materials is that the interface is then much more planar than when the FSP tool pin penetrates the bottom material (Fig. 1.18(b)). Indeed, the penetration of the tool inside the lower plate leads to material flowing upwards and thus a hooking effect [185, 186] sometimes degrading the mechanical properties due to local stress concentration [185] or, oppositely, improving the mechanical properties thanks to interlocking [186]. The assembly of large panels by classical friction stir lap welding is expected to lead to inhomogeneous microstructures, however this could be acceptable.

Constitutional liquation has been reported at the interface between two dissimilar metals when they present a low temperature eutectic among themselves. This is particularly the case for the Al-Mg system [187, 188] and has

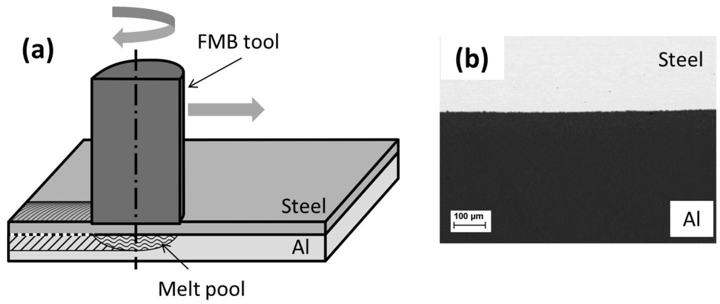

Fig. 1.19. (a) Principle of the friction melt bonding (FMB) process. (b) Planar interface between ULC steel and 1050 Al alloy in a friction stir melting joint (Courtesy of N. Jimenez-Mena).

also been reported for Al-Cu butt welds [189]. The Al-Mg phase diagram presents a eutectic phase at 450^{o}C while the FS temperatures can be much larger in particular for high rotational speeds [188]. This constitutional liquation may lead to the formation of solidification cracks that are evidently detrimental to the mechanical properties of the structure [188].

1.5 Porous architectured materials

1.5.1 Foam based structures

Hangai and co-workers [190–196] have extensively studied the possibility to make porous aluminum alloy based foam architectured structures by FSP. They have used FSP to finely distribute blowing agent (TiH_2) and pore stabilizing agent powder (Al_2O_3) inside an aluminum plate [190, 191]. The distribution of the foaming agent is ensured by passing over the stack with a FSP tool, see Fig. 1.20. The porosities are formed by a heat treatment after FSP. The foaming agent (here TiH_2) presents explosion hazards. Thus, foam was manufactured in cast Al alloys with no foaming agent, only the pore stabilizing agent was inserted by FSP in the Al plates [192, 194]. The foaming effect during the subsequent heat treatment is ensured by the gas pores and dissolved gas blown during casting. More finely distributed porosities were resulting from this modification of the process. In all cases the porosity content can be controlled by changing the holding time of the heat treatment after FSP [194]. The FSP step is needed to distribute homogenously the pore stabilizing agent.

Many graded or architectured structures have been processed using this technology. Fig. 1.21 shows some examples of these structures. Fig. 1.21(a) shows

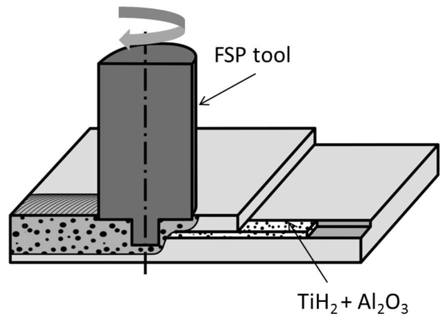

Fig. 1.20. Manufacturing process to make a foam by FSP (Schematic by N. Jimenez-Mena, inspired from Ref. [190]).

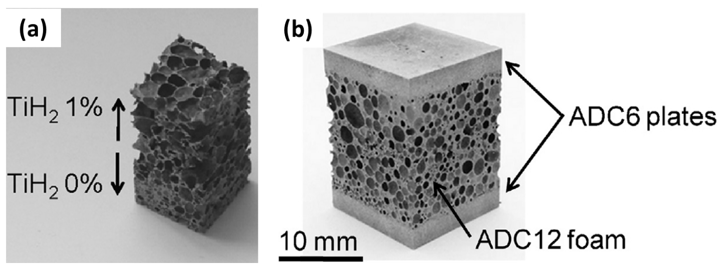

Fig. 1.21. Architectured structures based on aluminum foam made by FSP. (a) Graded porosities structure (from Hangai *et al.* [193]) and (b) sandwich structure fully assembled by FSP (no adhesive) (from Hangai *et al.* [194]).

an architectured material presenting a graded proportion of porosities [193]. This architectured material shows a good combination of compressive strength due to the low porosity part and compressive strain due to the high porosity part. Fig. 1.21(b) shows a sandwich panel made of ADC12 foam in between two dense ADC6 cast sheets [194]. Once more, the assembly is performed by FSP without the use of adhesive. This sandwich can thus be used for higher temperature applications. The formation of the sandwich rather than the foam alone provides higher tensile and bending strength. Hangai *et al.* [196] also developed by FSP graded foams composed of Al1050 and Al6061 foams produced by FSP separately and then assembled together by FSP. They showed that this assembly presents better compression and impact strain than the individual foams exploiting the prior deformation of the Al1050 foam followed by the deformation of the Al6061 foam.

1.5.2 Friction stir channeling

Balasubramanian *et al.* [197, 198] have invented a process derived from FSP called Friction Stir Channeling (FSC). FSC uses the large defect called worm-

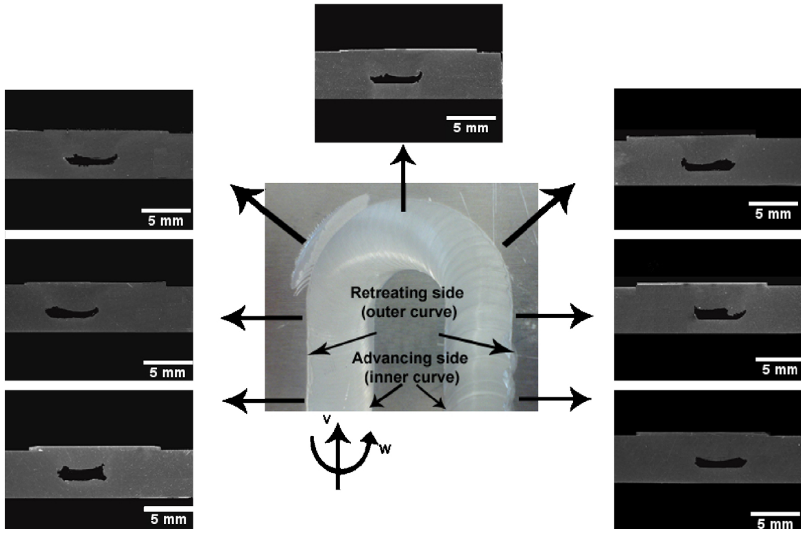

Fig. 1.22. Curvilinear channel processed by friction stir channeling. From Balasubramanian *et al.* [197].

hole formed for specific friction stir processing parameters to create channels with a path dictated by the FSC tool. This may, for example, be used to manufacture compact heat exchangers. Fig. 1.22 shows the typical shape of the channel that can be manufactured with a curvilinear path. The tool geometry, the process parameters and the applied force have to be correctly tailored in order for the channel to present a given shape and be continuous [197, 198].

1.6 Friction stir additive manufacturing

The additive manufacturing technology to process architectured materials is largely discussed in chapter **??**. Here, we will just shortly discuss the possibility of using the friction stir technology to perform additive manufacturing.

Friction Stir Additive Manufacturing (FSAM) is a very simple process using friction stir welding to assemble parts to build a 3D structure [199–201]. Fig. 1.23 presents the principle of this process. Small plates are lap jointed by FSW and may thus create a structure presenting the properties of the stir zone. Similarly to the laser cladding additive manufacturing process, this may help manufacture any structure with however limitations due to the need of a backing plate to support the load applied by the tool on the workpiece. Palanivel *et al.* [200] have shown that this technology may be applied to

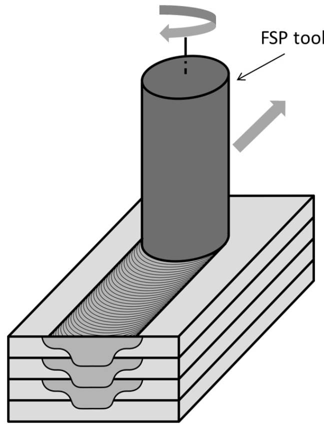

Fig. 1.23. Principle of friction stir additive manufacturing (Schematic by N. Jimenez-Mena, inspired from Ref. [201]).

process stringers for the skin panel of an airplane fuselage. The stringer is thus presenting the specific microstructure of an FSP material, contrarily to the skin panel.

Palanivel *et al.* [199,200] have made FSAM on a Mg-4Y-3Nd magnesium alloy. They found a high strength equal to 400 MPa with an excellent elongation of 17% due to the fine precipitates (2-7 nm) formed during a post-processing heat treatment. Yuqing *et al.* [201] show that the built microstructure presents some strong heterogeneities in an 7075 aluminum alloy.

References

1. W.M. Thomas, E.D. Nicholas, J.C. Needham, M.G. Murch, P. Templesmith, C.J. Dawes. GB patent application no. 9125978.8, December 1991; US patent no. 5460317, October 1995.
2. R.S. Mishra, M.W. Mahoney, S.X. McFadden, N.A. Mara, A.K. Mukherjee, Scripta Mater. **42**, 163 (2000)
3. R.S. Mishra, P.S. De, N. Kumar, Friction Stir Welding and Processing, Science and Engineering. (Springer, New York, 2014)
4. R.S. Mishra, Z.Y. Ma, Mater. Sci. Engin. R **50(1)** (2005) 1
5. M.-N. Avettand-Fènoël, A. Simar, R. Shabadi, R. Taillard, B. De Meester, Mat. Design **60**, 343 (2014)
6. J. Gandra, R. Miranda, P. Vilaa, A. Velhinho, J.P. Teixeira, J. Mater. Proc. Technol. **211**, 1659 (2011)

7. F.Khodabakhshi, A.Simchi, A.H.Kokabi, A.P.Gerlich, M.Nosko, Mater. Sci. Engin. A **642**, 204 (2015)
8. J.Q. Su, T.W. Nelson, C.J. Sterling, Scripta Mater. **52**, 135 (2005)
9. A.G. Rao, R.R. Ravi, B. Ramakrishnarao, V.P. Deshmukh, A. Sharma, N. Prabhu, B.P. Kashyap, Metall. Mater. Trans. A **44**, 1519 (2013)
10. N. Kumar, R.S. Mishra, Metall. Mater. Trans. A **44**, 934 (2013)
11. X. Feng, H. Liu, J.C. Lippold, Mater. Charact. **82**, 97 (2013)
12. C.G. Rhodes , M.W. Mahoney, W.H. Bingel, M. Calabrese, Scripta Mater. **48**, 1451 (2003)
13. A. Orozco-Caballero, P. Hidalgo-Manrique, C.M. Cepeda-Jimnez, P. Rey, D. Verdera, O.A. Ruano, F. Carreo, Mater. Charact. **112**, 197 (2016)
14. X.H. Du, B.L. Wu, Trans. Nonferrous Met. Soc. China **18**, 562 (2008)
15. J.A. del Valle, P. Rey, D. Gesto, D. Verdera, J.A. Jimnez, O.A. Ruano, Mater. Sci. Engin. A **628**, 198 (2015)
16. Jian-Qing Su, T.W. Nelson, T.R. McNelley, R.S. Mishra, Mater. Sci. Engin. A **528**, 5458 (2011)
17. A. Shafiei-Zarghani, Int. J. Modern Phys.B **22(18-19)**, 2874 (2008)
18. G.R. Cui, Z.Y. Ma, S.X. Li, Acta Mater. **57**, 5718 (2009)
19. M. Komarasamy, N. Kumar, Z. Tang, R.S. Mishra, P.K. Liaw, Mater. Res. Lett. **3(1)**, 30 (2015)
20. T. Morishige, T. Hirata, M. Tsujikawa, K. Higashi, Materials Let. **64**, 1905 (2010)
21. P. Xue, B.L. Xiao, Z.Y. Ma, Scripta Mater. **68**, 751 (2013)
22. T. Long, W. Tang, A.P. Reynolds, Sci. Technol. Weld. Join. **12** 311 (2007)
23. V. Kulitskiy, S. Malopheyev, S. Mironov, R. Kaibyshev, Mater. Sci. Engin. A **674**, 480 (2016)
24. N. Kumar, R.S. Mishra, C.S. Huskamp, K.K. Sankaran, Mater. Sci. Engin. A **528**, 5883 (2011)
25. K.A.A. Hassan, A.F. Norman, D.A. Price, P.B. Prangnell, Acta Mater. **51**, 1923 (2003)
26. M.A. Garcia-Bernal, R.S. Mishra, R. Verma, D. Hernandez-Silva, Mater. Sci. Engin. A **670**, 9 (2016)
27. I. Charit, R.S. Mishra, Scripta Mater. **58**, 367 (2008)
28. F. Hannard, S. Castin, E. Maire, R. Mokso, T. Pardoen, A. Simar, Acta Mater. **130**, 121 (2017)
29. S. Jana, R.S. Mishra, J.A. Baumann, G. Grant, Mater. Sci. Engin. A **528**, 189 (2010)
30. C.M. Hu, C.M. Lai, P.W. Kao, N.J. Ho, J.C. Huang, Scripta Mater. **60**, 639 (2009)
31. R. Kapoor, N. Kumar, R.S. Mishra, C.S. Huskamp, K.K. Sankaran, Mater. Sci. Engin. A **527**, 5246 (2010)
32. N. Kumar, R.S. Mishra, Mater. Sci. Engin. A **580**, 175 (2013)
33. B. Mansoor, A.K. Ghosh, Acta Mater. **60**, 5079 (2012)
34. J.G. Kaufman, E.L. Rooy, Aluminum AlloyCastings, Properties, Processes, and Applications (ASM International, U.S.A., 2004)
35. M.L. Santella, T. Engstrom, D. Storjohann, T.Y. Pan, Scripta Mater. **53**, 201 (2005)
36. Z.Y. Ma, S.R. Sharma, R.S. Mishra, Metall. Mater. Trans. A **37**, 3323 (2006)
37. Z.Y. Ma, S.R. Sharma, R.S. Mishra, Scripta Mater. **54** 1623 (2006)

38. Z.Y. Ma, S.R. Sharma, R.S. Mishra, Mater. Sci. Engin. A **433**, 269 (2006)
39. Z.Y. Ma, A.L. Pilchak, M.C. Juhas, J.C. Williams, Scripta Mater. **58**, 361 (2008)
40. A.H. Feng, B.L. Xiao, Z.Y. Ma, R.S. Chen, Metall. Mater. Trans. A **40**, 2447 (2009)
41. S. Jana, R.S. Mishra, J.A. Baumann, G.J. Grant, Metall. Mater. Trans. A **41**, 2507 (2010)
42. Z.W. Chen, F. Abraham, J. Walker, Mater. Sci. Forum **706-709**, 971 (2012)
43. S.S. Shin, E.S. Kim, G.Y. Yeom, J.C. Lee, Mater. Sci. Engin. A **532**, 151 (2012)
44. T.J. Hurley, R.G. Atkinson, Trans. Am. Foundry Soc. **91**, (1985) 29196
45. D.R. Ni, D. Wang, A.H. Feng, G. Yao, Z.Y. Ma, Scripta Mater. **61**, 568 (2009)
46. L. Karthikeyan, V.S. Senthilkumar, V. Balasubramanian, S. Natarajan, Mater. Design **30**, 2237 (2009)
47. K. Nakata, Y.G. Kim, H. Fujii, T. Tsumura, T. Komazaki, Mater. Sci. Engin. A **437**, 274 (2006)
48. S.R. Sharma, Z.Y. Ma, R.S. Mishra, Scripta Mater. **51**, 237 (2004)
49. P. Cavaliere, Materials Charact. **57**, 100 (2006)
50. S.R. Sharma, R.S. Mishra, Scripta Mater. **59**, 395 (2008)
51. S. Jana, R.S. Mishra, J.B. Baumann, G. Grant, Scripta Mater. **61**, 992 (2009)
52. S. Jana, R.S. Mishra, J.B. Baumann , G. Grant, Acta Mater. **58**, 989 (2010)
53. S.M. Aktarer, D.M. Sekban, O. Saray, T. Kucukomeroglu, Z.Y. Ma, G. Purcek, Mater. Sci. Engin. A **636**, 311 (2015)
54. S.A. Alidokht, A. Abdollah-Zadeh, S. Soleymani, T. Saeid, H. Assadi, Mater. Charact. **63**, 90 (2012)
55. S.K. Singh, R.J. Immanuel, S. Babu, S.K. Panigrahi, G.D. Janaki Ram, J. Mater. Proc. Technol. **236**, 252 (2016)
56. Z.Y. Ma, R.S. Mishra, M.W. Mahoney, Acta Mater. **50**, 4419 (2002)
57. I. Charit, R.S. Mishra, Mater. Sci. Engin. A **359**, 290 (2003)
58. Z.Y. Ma, R.S. Mishra, M.W. Mahoney , R. Grimes, Mater. Sci. Engin. A **351**, 148 (2003)
59. R.S. Mishra, Adv. Mater. Process. p.45 (Feb 2004)
60. Z.Y. Ma, R.S. Mishra, M.W. Mahoney, R. Grimes, Metall. Mater. Trans. A **36**, 1447 (2005)
61. Z.Y. Ma, R.S. Mishra, Scripta Mater. **53**, 75 (2005)
62. I. Charit, R.S. Mishra, Acta Mater. **53**, 4211 (2005)
63. F.C. Liu, Z.Y. Ma, Scripta Mater. **59**, 882 (2008)
64. Z.Y. Ma, R.S. Mishra, F.C. Liu, Mater. Sci. Engin. A **505**, 70 (2009)
65. M.A. Garcia-Bernal, R.S. Mishra, R. Verma, D. Hernandez-Silva, Scripta Mater. **60**, 850 (2009)
66. F.C. Liu, B.L. Xiao, K. Wang, Z.Y. Ma, Mater. Sci. Engin. A **527**, 4191 (2010)
67. Z.Y. Ma, F.C. Liu , R.S. Mishra, Acta Mater. **58**, 4693 (2010)
68. M.A. Garcia-Bernal, R.S. Mishra, R. Verma, D. Hernandez-Silva, Mater. Sci. Engin. A **534**, 186 (2012)
69. F.C. Liu, Z.Y. Ma, F.C. Zhang, J. Mater. Sci. Technol. **28(11)**, 1025 (2012)
70. A. Orozco-Caballero, M. Alvarez-Leal, P. Hidalgo-Manrique, C. M. Cepeda-Jimenez, O. A. Ruano, F. Carreno, Mater. Sci. Engin. A **680**, 329 (2017)
71. P. Cavaliere , P.P. De Marco, J. Mater. Process. Technol. **184**, 77 (2007)
72. D. Zhang, S. Wang, C. Qiu, W. Zhang, Mater. Sci. Engin. A **556**, 100 (2012)
73. F. Chai, D. Zhang, Y. Li, W. Zhang, Mater. Sci. Engin. A **568**, 40 (2013)

74. Q. Yang, B.L. Xiao, Q. Zhang, M.Y. Zheng, Z.Y. Ma, Scripta Mater. **69**, 801 (2013)
75. S.R. Babu, V.S.S. Kumar, L. Karunamoorthy, G.M. Reddy, Mater. Design **53**, 338 (2014)
76. S. Palanivel, A. Arora, K.J. Doherty, R.S. Mishra, Mater. Sci. Engin. A **678**, 308 (2016)
77. A. Simar, Y. Brechet, B. de Meester, A. Denquin, T. Pardoen, Acta Mater. **55**, 6133 (2007)
78. J.D. Robson, Acta Mater., Acta Mater. **52**, 1409 (2004)
79. C. Genevois., A. Deschamps, A. Denquin, B. Doisneau-Cottignies, Acta Mater. **53(8)**, 2447 (2005)
80. C. Gallais, A . Simar, D. Fabregue, A. Denquin, G. Lapasset, B. de Meester, Y. Brechet, T. Pardoen, Metall. Mater. Trans. A **38(5)**, 964 (2007)
81. A. Simar, Y. Brechet, B. de Meester, A. Denquin, T. Pardoen, Mater. Sci. Engin. A **486**, 85 (2008)
82. A. Simar, Y. Brechet, B. de Meester, A. Denquin, C. Gallais, T. Pardoen, Progress Mater. Sci. **57**, 95 (2012)
83. C.D. Marioara, S.J. Andersen, J. Janssen, H.W. Zandbergen, Acta Mater. **49**, 321 (2001)
84. M.-N. Avettand-Fènoël, R. Taillard, Metall. Mater. Trans. A **46(1)**, 300 (2015)
85. M.-N. Avettand-Fènoël, R. Taillard, Mater. Design **89c**, 348 (2016)
86. B.L. Xiao, Q. Yang, J. Yang, W.G. Wang, G.M. Xie, Z.Y. Ma, J. Alloys Compounds **509**, 2879 (2011)
87. A.M. Jamili, A. Zarei-Hanzaki, H.R. Abedi, P. Minarik, R. Soltani, Mater. Sci. Engin. A **690**, 244 (2017)
88. R.A. Seraj, A. Abdollah-Zadeh, M. Hajian, F. Kargar, R. Soltanalizadeh, Metall. Mater. Trans. A. **47**, 3564 (2016)
89. A.L. Pilchack, M.C. Juhas, J.C. Williams, Metall. Mater. Trans. A **38**, 401 (2007)
90. A.L. Pilchack, D.M. Norfleet, M.C. Juhas, J.C. Williams, Metall. Mater. Trans. A. **39**, 1519 (2008)
91. J.C. Lippold, J.J. Livingston, Metall. Mater. Trans. A **44**, 3815 (2013)
92. B. Li, Y. Shen, W. Hu, L. Luo, Surf. Coat. Technol. **239**, 160 (2014)
93. M. Sarkari Khorrami, M. Kazeminezhad, Y. Miyashita, A.H. Kokabi, Metall. Mater. Trans. A. **48**, 188 (2017)
94. G. Bhargava, W. Yuan, S.S. Webb, R.S. Mishra, Metall. Mater. Trans. A **41**, 13 (2010)
95. S. Mironov, Q. Yang, H. Takahashi, I. Takahashi, K. Okamoto, Y.S. Sato, H. Kokawa, Metall. Mater. Trans. A **41**, 1016 (2010)
96. R. Xin, B. Li, A. Liao, Z. Zhou, Q. Liu, Metall. Mater. Trans. A **43**, 2500 (2012)
97. W. Yuan, R.S. Mishra, B. Carlson, R.K. Mishra, R. Verma, R. Kubic, Scripta Mater. **64**, 580 (2011)
98. W. Yuan, R.S.Mishra, Mater. Sci. Engin. A **558**, 716 (2012)
99. V. Jain, R.S.Mishra, A.K.Gupta, Gouthama, Mater. Sci. Engin. A **560**, 500 (2013)
100. M. Vargas, S. Lathabai, P.J. Uggowitzer, Y. Qi, D. Orlov, Y. Estrin, Mater. Sci. Engin. A **685**, 253 (2017)
101. M.-N. Avettand-Fènoël, A. Simar, Mater. Charact. **120**, 1 (2016)
102. Y. Kimoto, T. Nagaoka, H. Watanabe, M. Fukusumi, Proc. 1st intern. Joint Symp. Join. Weld. 389 (2013)

103. A. Ghasemi-Kahrizsangi, S.F. Kashani-Bozorg. Surf. Coatings Technol. **209**, 15 (2012)
104. A. Shafiei-Zarghani, S. F. Kashani-Bozorg, A. Gerlich, Mater. Sci. Engin. A **631**, 75 (2015)
105. R.M. Miranda, T.G. Santos, J. Gandra, N. Lopes, R.J.C. Silva, J. Mater. Proc. Technol. **213**, 1609 (2013)
106. T.G. Santos, N. Lopes, M. Machado, P. Vilaa, R.M. Miranda, J. Mater. Proc. Technol. **216**, 375 (2015)
107. D. Lu, Y. Jiang, R. Zhou, Wear **305(1-2)**, 286 (2013)
108. E.R.I. Mahmoud, M. Takahashi, T. Shibayanagi, K. Ikeuchi, Wear **268**, 1111 (2010)
109. B. Li, Y. Shen, L. Luo, W. Hu, Mater. Sci. Engin. A **574**, 75 (2013)
110. M. Dixit, J.W. Newkirk, R.S. Mishra, Scripta Mater. **56**, 541 (2007)
111. S.R. Anvari, F. Karimzadeh, M.H. Enayati, J. All. Compnds. **562**, 48 (2013)
112. J. Gandra, P. Vigarinho, D. pereira, R.M. Miranda, A. Velhinho, P. Vilaa, Mater. Design **52**, 373 (2013)
113. A. Mertens, A. Simar, J. Adrien, E. maire, H.M. Montrieux, F. Delannay, J. Lecomte-Beckers, Mater. Charact. **107**, 125 (2015)
114. P. Liu, Q.Y. Shi, Y.B. Zhang, Composites: part B **52**, 137 (2013)
115. A. Shamsipur, S.F. Kashani-Bozorg, A. Zarei-Hanzaki, Surf. Coat. Technol. **218**, 62 (2013)
116. H. Eskandari, R. Taheri, Proc. Mater. Sci. **11**, 503 (2015)
117. Y. Morisada, H. Fujii, T. Nagaoka, M. Fukusumi, Mater. Sci. Eng. 433, 50 (2006b)
118. P. Asadi, G. Faragi, A. Masoumi, M.K.B. Givi, Met. Mater. Trans. 42A, 2820 (2011)
119. H. Izadi, A.P. Gerlich, Carbon **50**, 4744 (2012)
120. W. Yuan, R.S. Mishra, S. Webb, Y.L. Chen, B. Carlson, D.R. Herling, J. Mater. Process. Technol. **211**, 972 (2011)
121. R. Sathiskumar, N. Murugan, I. Dinaharan, S.J. Vijay, Mater. Charact. **84**, 16 (2013)
122. H. Sarmadi, A.H. Kokabi, S.M.S. Reihani, Wear **304**, 1 (2013)
123. V. Sharma, U. Prakash, B.V.M. Kumar, Mater. Today: Proceedings **2**, 2666 (2015)
124. D.R. Ni, J.J. Wang, Z.Y. Ma, J. Mater. Sci. Technol. **32(2)**, 162 (2016)
125. S. Soleymani, A. Abdollah-Zadeh, S.A. Alidokht, Wear **278-279**, 41 (2012)
126. C.J. Hsu, P.W. Kao, N.J. Ho, Mater. Letters **61**, 1315 (2007)
127. I.S. Lee, P.W. Kao, C.P. Chang, N.J. Ho, Intermetallics **35**, 9 (2013)
128. R. Bauri, D. Yadav, C.N.S Kumar, G.D.J. Ram, Data in Brief **5**, 309 (2013)
129. N. Yuvaraj, S. Aravindan, Vipin, J. Mater. Res. Technol. **4(4)**, 398 (2015)
130. M. Golmohammadi, M. Atapour, A. Ashrafi, Mater. Design **85**, 471 (2015)
131. Z.Y. Liu, B.L. Xiao, W.G. Wang, Z.Y. Ma, J. Mater. Sci. Technol. **30**, 649 (2014)
132. J.N. Aoh, C.W. Huang, W.J. Cheng, Mater. Sci. Forum **783-786**, 1721 (2014)
133. G.L. You, N.J. Ho, P.W. Kao, Mater. Charact. **80**, 1 (2013)
134. M. Sarkari-Khorrami, S. Samadi, Z. Janghorban, M. Movahedi, Mater. Sci. Engin. A **641**, 380 (2015)
135. M. Sarkari-Khorrami, M. Kazeminezhad, A.H. Kokabi, Met. Mat. Trans. A **46**, 2021 (2015)

136. S. Selvakumar, I. Dinaharan, R. Palanivel, B.G. Babu, Mater. Sci. Engin. A **685**, 317 (2017)
137. S. Fouladi, M. Abbasi, J. Mater. Proc. Technol. **243**, 23 (2017)
138. H. Eskandari, R. Taheri, F. Khodabakhshi, Mater. Sci. Engin. A **660**, 84 (2016)
139. C.N.S. Kumar, R. Bauri, D. Yadav, Tribology Intern. **101**, 284 (2016)
140. J.P. Oliveira, J.F. Duarte, P. Infacio, N. Schell, R.M. Miranda, T.G. Santos, Mater. Design **113**, 311 (2017)
141. N. Kumar, G. Gautam, R.K. Gautam, A. Mohan, S. Mohan, Tribology Intern. **97**, 313 (2016)
142. V.C. Gudla, F. Jensen, A. Simar, R. Shabadi, R. Ambat, Applied Surf. Sci. **324**, 554 (2015)
143. V.C. Gudla, K. Bordo, F. Jensen, S. Canulescu, S. Yuksel, A. Simar, R. Ambat, Surf. Coatings Technol. **277**, 67 (2015)
144. V. Sharma, U. Prakash, B.V. Manoj Kumar, J. Mater. Process. Technol. **224**, 117 (2015)
145. M. Barmouz, M.K. Besharati Givi, J. Seyfi, Mater. Charact. **62**, 108 (2011)
146. Y.F. Sun, H. Fujii, Mater. Sci. Engin. A **528**, 5470 (2011)
147. R. Sathiskumar, N. Murugan, I. Dinaharan, S.J. Vijay, Mater. Design **55**, 224 (2014)
148. T. Thankachan, K.S. Prakash, Mater. Sci. Engin. A **688**, 301 (2017)
149. M. Barmouz, P. Asadi, M.K. Besharati Givi, M. Taherishargh, Mater. Sci. Engin. A **528**, 1740 (2011)
150. Y. Jiang, X. Yang, H. Miura, T. Sakai, Rev. Adv. Mater. Sci. **33**, 29 (2013)
151. Y. Morisada, H. Fujii, T. Nagaoka, M. Fukusumi, Mater. Sci. Engin. **419**, 344 (2006)
152. M. Azizieh, A.H. Kokabi, P. Abachi, Mater. Design **32**, 2034 (2011)
153. C.J. Lee, J.C. Huang, P.J. Hsieh, Scripta Mater. **54**, 1415 (2006)
154. S.H. Abdollahi, F. Karimzadeh, M.H. Enayati, J. Alloys Compnds. **623**, 335 (2015)
155. D. Khayyamin, A. Mostafapour, R. Keshmiri, Mater. Sci. Engin. A **559**, 217 (2013)
156. D. Ahmadkhaniha, M. Fedel, M.H. Sohi, A.Z. Hanzaki, F. Deflorian, Corrosion Science **104**, 319 (2016)
157. M. Navazani, K. Dehghani, J. Mater. Proc. Technol. **229**, 439 (2016)
158. A. Shamsipur, S.F. Kashani-Bozorg, A. Zarei-Hanzaki, Surf. Coat. Technol. **206**, 1372 (2011)
159. S. Thapliyal, D.K. Dwivedi, J. Mater. Proc. Technol. **238**, 30 (2016)
160. G. Huang, Y. Shen, R. Guo, W. Guan, Mater. Sci. Engin. A **674**, 504 (2016)
161. Z. Du, M.J. Tan, J.F. Guo, G. Bi, J. Wei, Mater. Sci. Engin. A **667**, 125 (2016)
162. D. Ahmadkhaniha, P. Asadi, Mechanical alloying by friction stir processing, chap. 9, Advances in Friction Stir Welding and Processing, 387 (2014)
163. R.A. Prado, L.E. Murr, K.F. Soto, J.C. McClure, Mater. Sci. Engin. A **349**, 156 (2003)
164. H.J. Liu, J.C. Feng, H. Fujii, K. Nogi, Int. J. Machine Tools Manuf. **45**, 1635 (2005)
165. R.A. Prado, L.E. Murr, D.J. Shindo, K.F. Soto, Scripta Mater. **45**, 75 (2001)
166. K. Kalaiselvan, N. Murugan , Procedia Engin. **38**, 49 (2012)
167. S. Gopalakrishnan, N. Murugan, Mater. Design **32**, 462 (2011)
168. M. Barmouz, M.K. Besharati Givi, Composites: Part A **42**, 1445 (2011)

169. A. Simar, M.-N. Avettand-Fènoël, Sci. Technol. Welding Joining, dx.doi.org/10.1080/13621718.2016.1251712 (2016)
170. B. Li, Y. Shen, L. Luo; W. Hu, J. Alloys Compnds. **658**, 904 (2016)
171. F. Liu, Y. Ji, Q. Meng, Z. Li, Vacuum **133**, 31 (2016)
172. C. van der Rest, Dissertation, Université catholique de Louvain, Belgium (2015)
173. A. Elrefaey, M. Takahashi, K. Ikeuchi, J. Japan Welding Society **23**, 186 (2005)
174. Y.C. Chen, K. Nakata, Metall. Mater. Trans. A **39**, 1985 (2008)
175. R.S. Coelho, A. Kostka, S. Sheikhi, J.F. dos Santos, A.R. Pyzalla. Adv. Engin. Mater. **10**, 961 (2008).
176. M. Haghshenas, A. Abdel-Gwad, A.M. Omran, B. Gke, S. Sahraeinejad, A.P. Gerlich, Mater. Design **55**, 442 (2014).
177. Y.C. Chen, K. Nakata, Mater. Design **30**, 469 (2009)
178. M. Aonuma, K. Nakata, Mater. Sci. Engin. B **173**, 135 (2010)
179. M.N. Avettand-Fènoël, R. Taillard, G. Ji, D. Goran, Metall. Mater. Trans. A **43**, 4655 (2012)
180. J.T. Xiong, J.L. Li, J.W. Qian, F.S. Zhang, W.D. Huang, Sci. Technol. Welding Joining **17**, 196 (2012).
181. C. Schneider, T. Weinberger, J. Inoue, T. Koseki, N. Enzinger, Sci. Technol. Welding Joining **16**, 100 (2011).
182. G. Zhang, W. Su, J. Zhang, Z. Wei, Metall. Mater. Trans. A **42**, 2850 (2011)
183. C. van der Rest, P.J. Jacques, A. Simar, Scripta Mater. **77**, 25 (2014)
184. S. Crucifix, C. van der Rest, N. Jimenez-Mena, P.J. Jacques, A. Simar, Sci. Technol. Welding Joining **20**, 319 (2015)
185. S. Jana, T. Hovanski, Sci. Technol. Welding Joining **17**, 141 (2012)
186. J. Mohammadi, Y. Behnamian, A. Mostafaei, H. Izadi, T. Saeid, A.H. Kokabi, A.P. Gerlich, Mater. Charact. **101**, 189 (2015)
187. Y.C. Chen, K. Nakata, Scripta Mater. **58**, 433 (2008)
188. J. Yan, Z. Xu, Z. Li, L. Li, S. Yang, Scripta Mater. **53**, 585 (2005)
189. J. Ouyang, E. Yarrapareddy, R. Kovacevic, J. Mater. Process. Technol. **172**, 110 (2006)
190. Y. Hangai, M. Hasegawa, T. Utsunomiya, J. Mater. Process. Technol. **210**, 288 (2010)
191. Y. Hangai, Y. Oba, S. Koyama, T. Utsunomiya, Metall. Mater. Trans. A **42**, 3585 (2011)
192. Y. Hangai, H. Kato, T. Utsunomiya, S. Kitahara, O. Kuwazuru, N. Yoshikawa, Mater. Trans. **53(8)**, 1515 (2012)
193. Y. Hangai, K. Takahashi, T. Utsunomiya, S. Kitahara, O. Kuwazuru, N. Yoshikawa, Mater. Sci. Engin. A **534**, 716 (2012)
194. Y. Hangai, H. Kamada, T. Utsunomiya, S. Kitahara, O. Kuwazuru, N. Yoshikawa, J. Mater. Process. Technol. **214**, 1928 (2014)
195. Y. Hangai, K. Saito, T. Utsunomiya, O. Kuwazuru, N. Yoshikawa, Mater. Sci. Engin. A **613**, 163 (2014)
196. Y. Hangai, N. Kubota, T. Utsunomiya, H. Kawashima, O. Kuwazuru, N. Yoshikawa, Mater. Sci. Engin. A **639**, 597 (2015)
197. N. Balasubramanian, R.S. Mishra, K. Krishnamurthy, J. Mater. Process. Technol. **209**, 3696 (2009)
198. N. Balasubramanian, R.S. Mishra, K. Krishnamurthy, J. Mater. Process. Technol. **211**, 305 (2011)
199. S. Palanivel, P. Nelaturu, B. Glass, R.S. Mishra, Mater. Design **65**, 934 (2015)

200. S. Palanivel, H. Sidhar, R.S. Mishra, JOM **67(3)**, 616 (2015)
201. M. Yuqing, K. Liming, H. Chunping, L. Fengcheng, L. Qiang, Int. J. Adv. Manuf. Technol. doi10.1007/S00170-015-7695-9 (2015)